https://dx.doi.org/10.1016/j.compscitech.2021.108729

Permeable and washable electronics based on polyamide fibrous membrane for wearable applications

Su Yang[a], Su Liu[a], Xujiao Ding[a], Bo Zhu[b], Jidong Shi[c], Bao Yang[a], Shirui Liu[a], Wei Chen[a], Xiaoming Tao[a]*

[a] Research Centre for Smart Wearable Technology, Institute of Textiles and Clothing, The Hong Kong Polytechnic University, Hong Kong, 999077, China

[b] College of Professional and Continuing Education, The Hong Kong Polytechnic University, Hong Kong, 999077, China

[c] College of Engineering Physics, Shenzhen Technology University, Shenzhen 518118, China

Abstract:

Integrating electronics in clothing is a significant milestone of wearable technology. The priority is to develop flexible interconnector with great washability, durability and comfort wearability. In this work, we reported an air-permeable and machine-washable Cu/Ni interconnector based on highly flexible fibrous polyimide (FPI) membrane. Benefiting from the porous merit of FPI membrane and robust parylene encapsulation, the novel interconnector presents excellent conductivity (14 mΩ/sq), decent air-permeability (11 KPa*s/m) and superior electromechanical stability after abrasion of 50000 cycles, bending of 10000 cycles, and machine washing of 50 times. Moreover, assemblies made from the FPI-based circuit board not only show desirable lifespan in harsh environments, including seawater, ice, boiled water, and heavy rain, but also can be woven into fabrics for broad wearable applications. The work presents a facile and effective method to fabricate highly flexible, comfortable and durable interconnector, guaranteeing the reliability for long-term wearable application and showing great possibility for high-throughput production.

Keywords: Wearables, Interconnector, Washability, Fibrous membrane

1. Introduction

With the advance of materials and microelectronic integration technology, modern electronics are moving toward an emerging field of wearable systems. Up to now, wearable electronics have found extensive applications in various fields, such as flexible displays,[1] health monitoring, [2, 3] human-machine interaction,[4] electronic skins,[5, 6] and many others.[7, 8] With the final goal of integrating electronic circuits with our clothing, continuous efforts are geared towards constructing wearable electronics with lightweight, highly reliable, durable, comfortable, even imperceptible for the user, which is still a huge challenge since wearable comfort and reliability always compromise.[9]

In this scenario, the primary target is to develop reliable and highly conductive interconnector, which serves as an indispensable component to connect different electronic components. Generally, the majority of reported flexible interconnectors are fabricated based on two-dimensional (2D) polymer films because of their great compatibility with different electronic components and extremely high stability.[10, 11] When taking the human-centric point of comfortability and wearability into account, fibrous membranes with air permeable merits and superior tear strength would be eligible alternatives to explore high-quality interconnector meanwhile maintain comfortable wearability. [12] Fibrous structure is beneficial to suffer from repetitive stresses during daily tear of garments and avoid stuffy feeling and even inflammation of skin. Fibrous membranes like papers and electrospun membranes have been employed to fabricate flexible interconnectors. For example, flexible interconnectors based on printing paper,[13] tissue paper, [14] brochure paper, [15] and air-laid paper [16] have been widely reported. Nevertheless, limited by weak wet strength, most paper-based interconnectors were functioned as one-time disposable electronics. Besides, the fabrication process is mainly limited by various physical methods such as writing, printing, vaporization, vacuum filtration,[17] while there is very little report about using the industrial and commercial solution-based methods like chemical plating and electroplating. On the other hand, highly flexible interconnectors based on electrospun membranes have been recently reported, which could be further applied for strain sensors or chemical vapor sensors.[18-20] However, the time-consuming and complicated preparation process have greatly restricted their large-scale production. Thereupon, it is urgently needed to find one new fibrous membrane to construct highly conductive and durable interconnector with decent wearability and scalable fabrication.

Primarily designed for wearable applications, such reliable interconnector is highly desirable to be electro-mechanically durable and machine-washable. It places the demand that the flexible interconnectors are

capable of keeping the stable conductivity during the synchronous deformations with human body, such as bending, friction and twisting.[21] Up to now, flexible interconnectors based on fibrous membranes still suffer from undesirable electro-mechanical durability. For example, the limited bending cycles result in multifold increase of resistance.[22] And obvious cracks were developed under large deformation.[23] On the other hand, machine-washability is also an intractable issue for wearable interconnectors, which places higher stability requirement for the interconnectors to stand up to the intense spinning/friction and water invasion during machine washing.[24-26] Nevertheless, most of reported washable interconnectors possess limited machine-washing cycles but high relative resistance change. [27, 28] Besides, the machine-washability of flexible interconnector based on fibrous membrane has seldom been addressed in previous works. Furthermore, in daily using the interconnectors will also face different working environment, such as low/high temperature, humid, and acid/alkaline liquids, hence an anticorrosive performance is also of great importance for the practical applications to avoid the external corrosion.[13] Thus, it is crucial to explore a simple and efficient strategy to improve the durability and washability of the flexible interconnectors based on fibrous membrane, meanwhile without sacrificing the wearable comfort.

In this contribution, to address the above challenges, a highly conductive, stable, and wearable interconnector with multilayered structure was elaborately designed and fabricated, with the unique fibrous polyimide (FPI) membrane as substrate, highly conductive alloy of Cu/Ni as conductive materials, and robust and nano-sized parylene as encapsulation layer. The FPI membrane possesses high thermal and dimensional stability, excellent dielectric properties, weather resistance and wet strength, which guarantees resultant interconnector safe and reliable performance during fabrication and long-term applications. In addition, of great interest is its porous feature and soft hand-feeling compared with the common film counterpart. On the other hand, benefiting from the thin but robust encapsulation by parylene, the encapsulated interconnector still presents high flexibility, good air-permeability, and fascinating electromechanical stability after abrasion of 50000 cycles, bending of 10000 cycles, and machine washing of 50 times. Furthermore, as a proof of concept, a simple flexible circuit board (FCB) was further fabricated by soldering a series of LEDs on the interconnectors, followed by parylene encapsulation. The high thermal stability of FPI membrane assures the smooth soldering process under high temperature. Thanks to robust interconnector and all-pervasive protection of parylene encapsulation, the FPI-based electronics display outstanding working stability under various harsh environment conditions, including seawater, ice/boiling water, and heavy rainy days. More importantly, the FPI electronics presents good tailorability and integration ability, which can be easily minimized to be incorporated into textile by simple braiding or

weaving, meanwhile with little influence on the aesthetic beauty and comfortable wearing of textiles, showing huge potential for the wearable electronics applications.

2. Experimental section

2.1. Materials

FPI membrane with 90 μm thickness was purchased from Changchun Gao Qi polyimide material Co., Ltd, China. Monochloro-p-xylene (C powder) was bought from A Cookson Electronics Company, USA. $SnCl_2$, $PdCl_2$, $NiCl_2$, and HCl were kindly provided by Dieckman chemical industry co. LTD, Hong Kong. Commercially nickel (Ni)-plating bath solutions were purchased from A&D (Asia Pacific) Company Limited, Hong Kong. Non-cyanide alkaline copper (Cu) plating solution was purchased from Sun Wing Technology Company, Hong Kong. Ni strike plating solution was made in lab (adding 240 g $NiCl_2$ (Vale Inco, Canada) and 120 mL 37 % HCl into 1 L deionized water). Photo resist film FF-9040S was purchased from Chang Chun Chemical Co., Ltd, China.

2.2. Metal deposition on FPI membrane

The preparation of conductive FPI membrane includes electroless plating of Ni, electroplating of Cu and Ni, respectively. The electroless Ni plating was completed by three steps of sensitization, activation, and deposition. In details, a piece of FPI membrane was firstly immersed into $SnCl_2$ solution for 5 min and $PdCl_2$ solution for 3 min at room temperature orderly, followed by activation in 5 % H_2SO_4 for 5 min at 50 ^oC. Flushing with mass of deionized water was involved after each step. Then, the above FPI membrane was put into Ni plating bath at 35 ^oC for 5 min. At last, the electroplating of Cu and Ni was successively finished for 20 min and 1.5 min. The resultant sample is short-named as metal-FPI. As for the FCB, the metal pattern was completed by a photolithography process, and then the light-emitting diodes (LEDs) were surface mounted with the assistance of soldering tin. The soldering temperature was 280 ^oC.

2.3. Encapsulation process

The parylene deposition was implemented by Parylene Deposition System (SCS PDS2010E LABCOTER). Before encapsulation, the samples were vertically mounted and hung on a homemade supporting frame for complete and uniform encapsulation. A glass slide was put on the bottom of the frame to measure the

deposited thickness of parylene film. Parylene deposition process mainly involves three steps: vaporization of dimer precursor at 175 °C, pyrolysis of dimer into its monomeric form (para-xylene) at 690 °C, and deposition of transparent parylene on targets' surfaces under vacuum of 60 mTorr (**Scheme S1**). The addition of monochloro-p-xylene is controlled as 22 g for once deposition. For brevity, the final sample of parylene-metal-FPI membrane was named as PMP.

2.4. Integration within textile process

The first step was yarn spinning. As-fabricated flexible electronics were cut into strips, which served as core yarns. Wrapping by polyethylene as loading yarn and nylon 6 as cover yarn, the electronic yarns were spun by home-made yarn manufacture machine (**Scheme S2**). The second step was integration within textile. The electronic yarns were braided as wearable bracelet for decoration and washing test. Furthermore, the electronic yarns were woven into fabrics by weaving machine (AVL Studio Doddy Loom) with plain weave structure.

2.5. Characterization and evaluation

2.5.1. Physical test: Electric conductance of metal-FPI after electroless plating and electroplating was tested by four-point probe (ST2258A, Suzhou Jingge Electronic Co., LTD, China). Scanning electron microscope (SEM, including TM3000 Hitachi, Japan and VEGA3 TESCAN, Czech) and energy dispersive X-ray spectroscopy (EDS) was employed to study the morphology change and element analysis after tension, abrasion and washing. The air permeability impedance was tested by automatic air-permeability tester, KES-F8-AP1, KATO TECH CO,.LTD). Thermo-gravimetric analysis (TGA, Mettler Toledo DSC/TGA1, Switzerland) was applied to test the thermal stability by heating from 50 to 1000 °C at a heating rate of 10 °C/min under nitrogen atmosphere. The thickness of parylene was decided by Dektak XT Surface optical profiler (Bruker, USA). The tensile properties of different samples were measured with a tensile rate of 20 mm/min by Instron 5944, USA. The gauge length of tension was 10 cm and sample size of 25 cm × 15 mm. Abrasive resistance is an important factor to judge the abrasion durability of the interconnector, which was measured by Martindale Abrasion Tester according to ASTM D4966-98.

2.5.2. Electro-mechanical test: For bending and machine-washing tests, the samples have a size of 80 mm × 5 mm. I-V characteristics of the PMP interconnector at different bending degrees with the gauge length of 40 mm were detected by Keithley 2400 (Tektronix, USA). Cyclic bending test was implemented by Instron 5944, with Keithley 2010 recording the resistance change simultaneously. The finite element

analysis (FEA) simulation of voltage drop was conducted by COMSOL, which was employed to analyze cracks development on resistance change of the interconnector during bending. In details, the SEM image was firstly vectorized, and then a potential difference of 1 V was applied on both left and right sides as the boundary conditions. The upper and lower boundaries were of insulation. For the materials parameters, the metal conductive area was assigned with the conductivity of 6×10^{7} S/m, while the crack area was defined with a low value of 1×10^{-6} S/m. Then potential distribution was calculated.

2.5.3. Washing test: Machine washing tests of metal-FPI and PMP were conducted with a washing machine (3LWTW4815FW, Whirlpool, USA) according to AATCC standard TS-007 with 66 g AATCC standard detergents for each cycle. In detail, the samples were put into a laundry bag along with 1.8 kg cotton fabrics as ballast. The washing cycle involved washing, rinsing, spinning and drum drying. A single washing time was 30 min at 40 ºC, followed by drum drying for 1 hour. For perspiration test, the artificial sweat with pH 8.0 was synthesized by 0.5 g/L $C_6H_9O_2N_3.HCl.H_2O$, 5 g/L NaCl, 5 g/L $Na_2HPO_4.12H_2O$, 2.5 g/L $Na_2HPO_4.2H_2O$, and 0.1 mol/l NaOH. Samples were immersed in the artificial sweat for 5 h at 37 ºC and dried overnight according to ISO 105-E04:2013. Forward Looking Infra-Red camera (E33, FLIR, USA) was used to capture the working temperature of LEDs for 90 days. Hand washing has been conducted according to AATCC LP2-2018.

3. Results and discussion

3.1. Fabrication process

The detailed process for preparing PMP interconnector was described in **Fig. 1**. In this process, electroless plating and electroplating were applied together to transform FPI substrate from insulating into highly conductive (**Fig. 1a**). Electroless plating is very useful for electrically functionalization of insulating substrate and electroplating has the advantages of easily controlled thickness and rapid speed.[29] Three metal layers, including electroless Ni plating, electroplating Cu as well as Ni were successively performed. It is well known that Cu-Ni plating multilayers possess good mechanical, electrical properties, and long-term reliability.[30] The first step is electroless plating Ni instead of Cu, because photo resist film used in the patterning cannot withstand high alkaline of electroless Cu plating solution. Thanks to fibrous surface of FPI membrane, substantial Ni particles were easily absorbed on the substrate by electroless plating (sheet resistance about 5.0 Ω/sq), which can act as metal crystal nucleus to initiate the following Cu electroplating. Secondly, electroplating Cu and Ni were implemented orderly to further enhance the conductivity

meanwhile improve their oxidation resistance. The final sheet resistance of interconnector was only about 14 mΩ/sq. Thirdly, to protect interconnector from external damage, the metal coated samples were vertically mounted on a homemade supporting frame for complete parylene encapsulation (**Fig. 1b**).

In detail, as a typical chemical vapor deposition process, parylene dimer precursor was firstly vaporized and pyrolyzed into its monomers at high temperature (**Scheme. S1**). These gaseous monomers were evenly distributed into the whole chamber and able to easily permeate into porous metal-FPI. With the assistance of three-dimensional (3D) supporting frame, parylene monomer possesses equal opportunity to access to suspended metal-FPI from all directions, not just one side. And then parylene precursors self-assemble into a 3D continuous and pinhole-free parylene protective layer, enwrapping porous metal-FPI from the inside out. Taken one metal-FPI fiber as example, the parylene film forms a conformal coating on metal-FPI fiber by virtue of ubiquitous gas-phase deposition at the molecular level as delineated in the insert (**Fig. 1b**). Furthermore, the EDS mapping was implemented to examine the element distribution on the cross section of PMP. It is saliently displayed that Cl element evenly distributes the entire cross section of PMP. That means parylene not only fully covers on the surface but also infiltrates into the interstitial gaps of metal-FPI, forming a 3D encapsulation structure rather than two simple layers covering on the top and bottom surfaces. Such hierarchical structure provides the highly pervasive protection for the PMP interconnector by parylene.

The sample photo of PMP interconnector shows similar flexibility and appearance with unencapsulated one, both of which can be easily lifted by leaves, indicating the maintaining of light-weight feature (**Fig. 1a**). The porosity and the roughness of FPI membrane increases the difficulty to measure the thickness of parylene directly. Herein, the thickness of parylene deposited on glass slide is calculated as ca. 6 μm (**Fig. S1c**) as a reference. More importantly, such hierarchical structure endows the interconnector with decent air permeability, despite the specific airflow resistance of PMP interconnector increases from 6 to 11 KPa*s/m compared with unencapsulated one. It manifests that PMP interconnector is air permeable due to epitaxial growing feature of parylene, which is totally different with the complete filling of all the interstitial spaces by polydimethylsiloxane encapsulation. It is anticipated that compact parylene encapsulation can improve waterproof properties and maintain high electrical stability of PMP interconnector under different working environments, meanwhile without losing its air permeability.

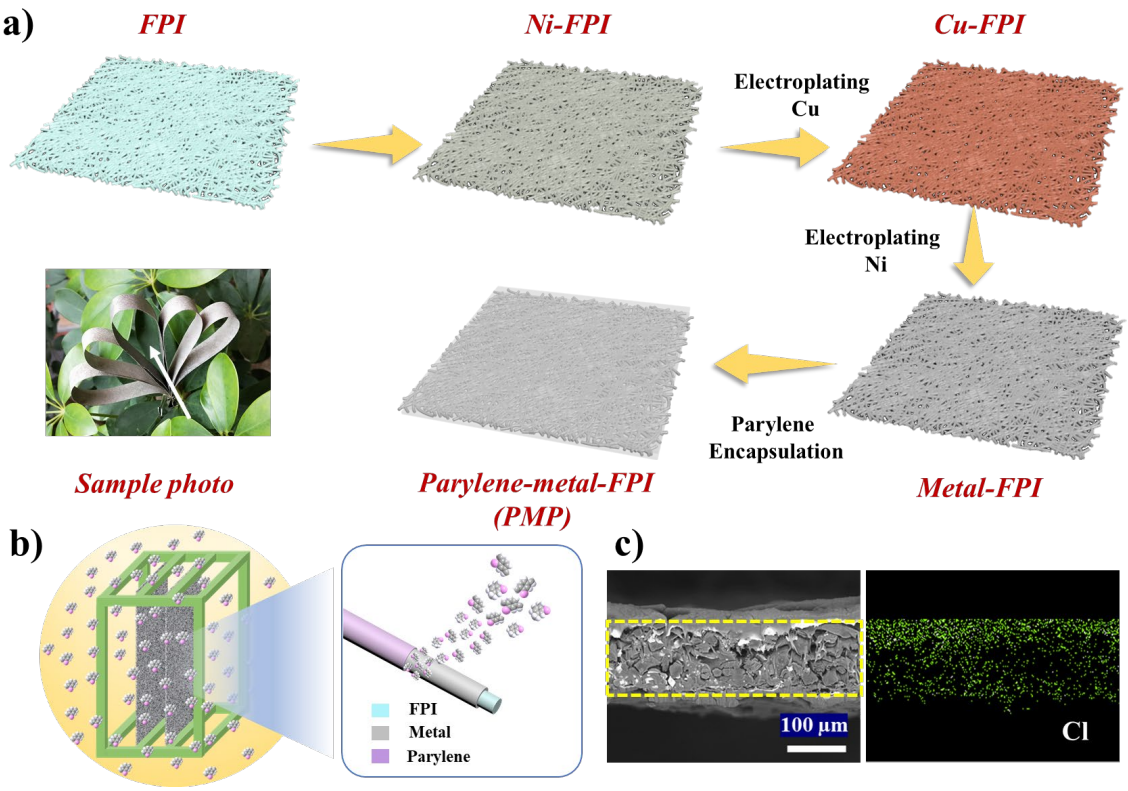

Fig. 1. Schematic illustration of the fabrication process. (a) PMP preparation process and sample photo, the white arrow points to the PMP. (b) The parylene deposition on Metal-FPI fixed on 3D printed supporting frame. The insert displays ubiquitous feature of parylene encapsulation. (c) SEM cross section of PMP as well as the related EDS mapping.

3.2. Morphologies and tensile properties

The optical images and SEM images give us direct impression on the structure development during the preparation process. As shown in **Fig. 2a**, FPI membrane features abundant long fibers and a small part of short fibers, showing a paper-like structure. The surface roughness is about 3.9 μm and water contact angle is about 90° (**Fig. S1**). The interlaced structures of FPI membrane provide multiple interstitial channels to allow air penetrating. Highly conductive metals are successfully deposited on the surface of FPI membrane with abundant Ni and Cu (**Fig. 2b**). The relative weight ratio of Ni and Cu occupies 20.2 % and 69.5 %, respectively (**Fig. S3**), despite a small amount of metals dispersed into large gap between FPI fibers (**Fig. S2**). It is known that the higher electrical conductivity positively depends on more conductive paths. The dense metal-covered FPI membrane constitutes of ample conductive paths from both sides, which guarantees the high and stable conductivity. It is worth noting that there still exists plenty of porous features

from the top view of PMP after metal deposition and parylene coating (**Fig. 2c**), which retains the air-permeability feature. The similar optical morphology appears on PMP interconnector because of transparent encapsulation (**Fig. 2c**). The SEM image of PMP in the insert **Fig. 2c** demonstrates the conformal coating feature of parylene based on fibrous contours, which is different from polydimethylsiloxane coating to fully cover all interspace. From the DES analysis of the top view of PMP in **Fig. 2d**, it is clearly shown that C and Cl elements dominate on the surface of PMP, further confirming the compact parylene encapsulation is successfully accomplished on PMP.

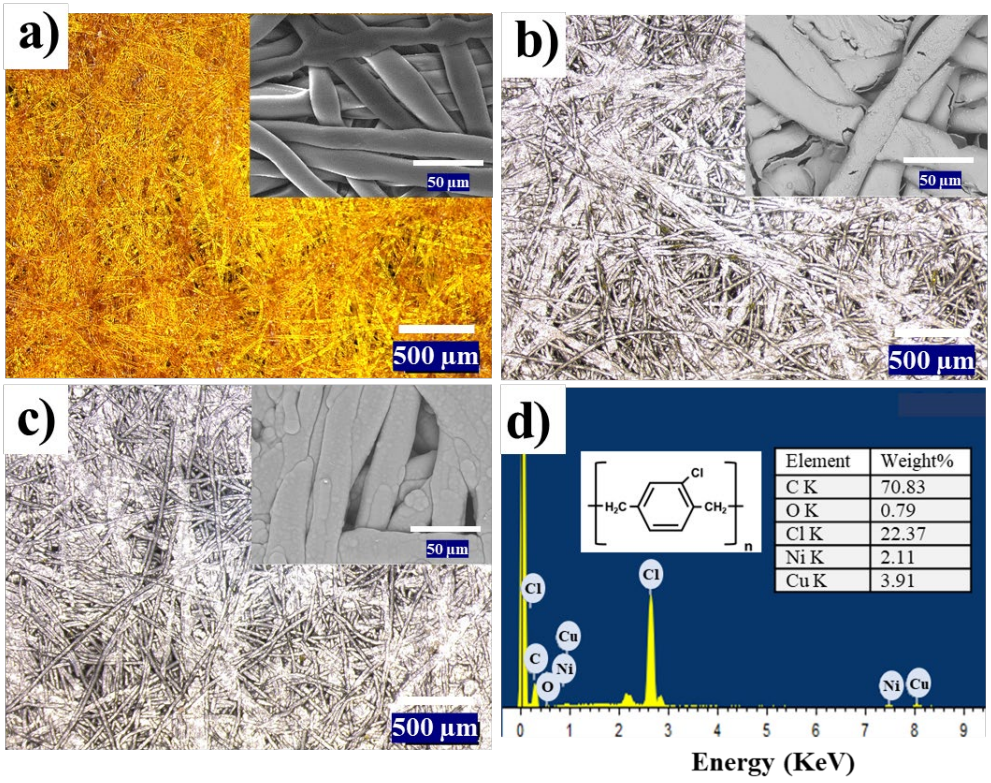

Fig. 2. The morphologies. The top view optical images of (a) FPI membrane, (b) Metal-FPI, (c) PMP. The inserts are zoom-in SEM images. (d) The EDS analysis of the top view of PMP.

The tensile properties were tested to study the effect of metal deposition and parylene encapsulation. As depicted in **Fig. 3a**, pure FPI presents a tensile strength of 8.7 MPa and Young's modulus of 652.2 MPa as well as elongation at break of 2.5 %. Strong metal layer can enhance tensile strength and Young's modulus of metal-FPI. Furthermore, PMP shows great increase by 67 % and 64 % in tensile strength and Young's modulus than unencapsulated one, which indicates that compact parylene encapsulation exerts positive influence on tensile properties of metal-FPI. From the cross-sectional SEM images after tension, loose

structure is clearly observed in the cross section of FPI membrane after tension, with abundant fiber-fiber interfacial debonding and fiber pull-out (**Figure 3b**). In clear contrast, PMP interconnector becomes much more compacted after tension (**Fig. 3d**), which gives plausible explanation of enhanced mechanical properties. On one side, the ubiquitous parylene encapsulation is beneficial to get more compact and integral structure to enhance the tensile strength of PMP. On the other side, it is reported that the modulus of parylene reached 2-5 GPa [31], which is much larger than that of metal-FPI here (1.3 GPa). Hence, parylene as strengthening agent improves the modulus of PMP in our work. The thermal properties of PMP interconnector were also detected by TGA. Pure FPI membrane remains stable before 497.0 ºC and metal-FPI starts to degrade at 502.7 ºC (**Fig. S3**). Parylene film also shows high starting thermal degradation temperature of 476.0 ºC (listed in **Table S1**). Such high degradation temperature guarantees the smooth soldering of LEDs as mentioned in experimental section, where soldering temperature is high up to 280 ºC. Based on ubiquitous parylene encapsulation as well as mechanical strengthening effects, it is well envisioned that PMP interconnector is capable of withstanding complicated deformations and washing damage, meanwhile maintaining high conductivity.

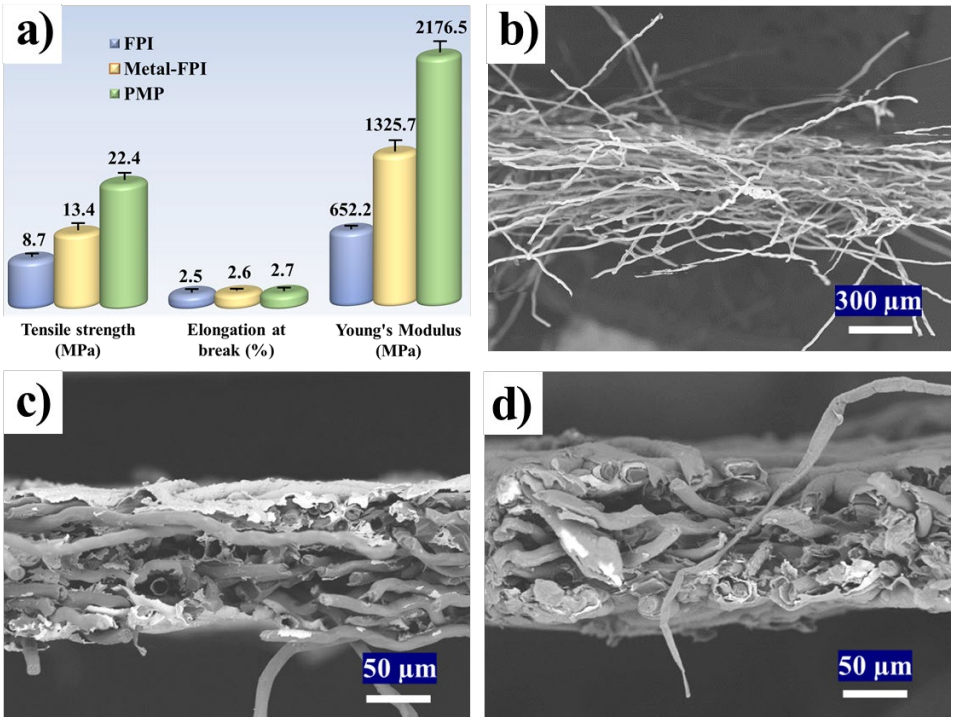

Fig. 3. The tensile properties. (a) The tensile properties of FPI, Metal-FPI and PMP. The SEM cross section of (b) FPI, (c) Metal-FPI and (d) PMP after tension.

3.3 Electromechanical durability

High abrasion resistance and cyclic bending are very important for wearable electronics, concerning long wearing and tearing in daily use. In **Fig. 4a**, up to 32 % mass loss is displayed for pure FPI after abrasion of 2000 cycles. The surface of pure FPI membrane has been severely worn in the abraded parts as shown in **Fig. 4c**. It is not surprising that metal-FPI shows better abrasion resistance than FPI membrane since Ni layer is well-known for excellent wear performance.[32] However, 12 % mass loss ratio of metal-FPI is still tracked on account of the weak interface between metals and FPI membrane as well as intrinsically poor abrasion resistance of FPI membrane. It is observed clearly that large area of metal has been stripped (**Fig. 4d**). What's stirring is that PMP interconnector exhibits supreme abrasive endurability in contrast with unencapsulated counterpart. There is only a little amount of mass loss ratio (2.2 %) and the surface almost keeps intact after 50000 cycles (**Fig. 4e**). EDS is employed to detect the change of Ni/Cu weight ratio. The result shows that the Ni/Cu weight ratio of metal-FPI obviously decreases from 0.82 to 0.67 after abrasion. In clear contrast, that of PMP interconnector yields little change after abrasion (**Fig. 4b**), fully satisfying the practical wearable requirement. The PMP interconnector demonstrates satisfactory abrasion resistance owing to compact parylene encapsulation, which maybe attribute to the strengthened and compact structure between the conductive layer and flexible substrate. It can be further confirmed by peeling strength test by 3M tape, where delaminated metals are observed on 3M tape for unencapsulated one. In clear contrast, there is no metal peeling from PMP interconnector (**Fig. S4**).

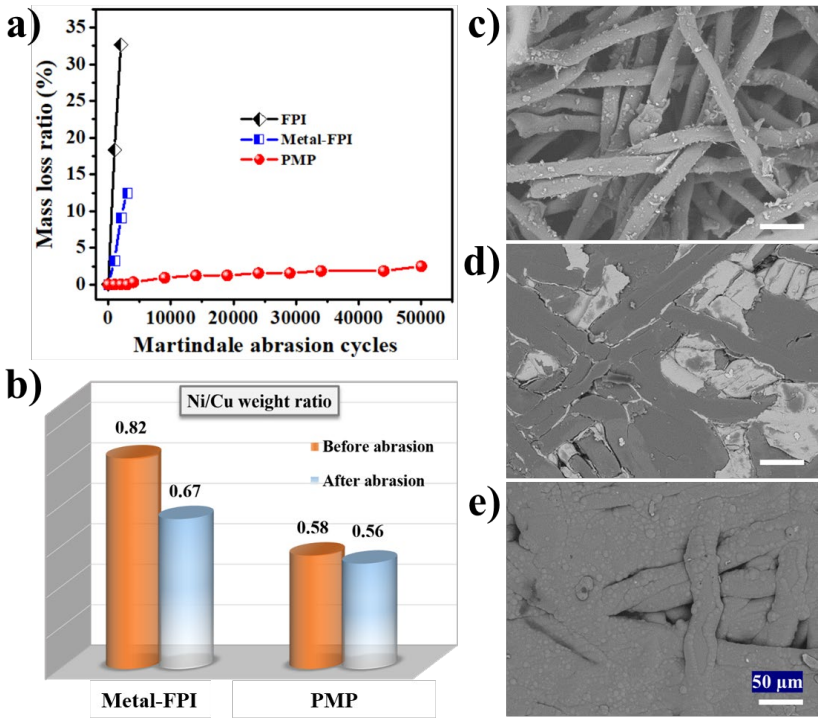

Fig. 4. The abrasion resistance. (a) The mass loss ratio against Martindale abrasion cycle for PMP. (b) The EDS result about weight ratio change of Ni/Cu for Metal-FPI and PMP before abrasion and after abrasion. (c) The SEM surface morphology of FPI membrane after 2000 cycles abrasion. (d) The SEM image of metal-FPI after 2000 cycles abrasion. (e) The SEM image of PMP after 50000 cycles abrasion.

As depicted in **Fig. 5a**, both metal-FPI and PMP display repeatable linear current-voltage characteristics at different static bending curvature radii, indicating the ohmic behavior of PMP interconnector with stable conductivity. The bending curvature radius (r) is calculated as following equation: $c = 2r*\sin(l/2r)$, where c is chord length and l is arc length.[33] To further investigate their dynamic bending reliability, PMP interconnector is actuated from flat to bent states at the same bending curvature radius of 1.0 cm. Relative resistance change ($\Delta R/R_0$) has been recorded simultaneously for every bending cycle. The result in **Fig. 5b** shows metal-FPI and PMP experience rapid increase of $\Delta R/R_0$ firstly and reaches a slowly increased plateau after ca. 2000 cycles. More notably, PMP interconnector owns prominent bending durability with only 13.2 % of $\Delta R/R_0$ increase over 10000 dynamic cycles, mainly thanks to the alleviation of parylene film. For unencapsulated counterpart, a slightly larger increase of $\Delta R/R_0$ (44.3 %) has been reflected (**Fig. 5b**). Besides, for each bending cycle with a certain frequency, a regular response curve is generated for both metal-FPI and PMP. Regular fluctuations range of PMP interconnector is obviously smaller than that of

metal-FPI as compared with the inserted curves in **Fig. 5b**, suggesting a more stable PMP interconnector than unencapsulated one. Such small fluctuations can be ignored because of high conductivity of PMP interconnector.

To investigate the underpinning mechanism of the $\Delta R/R_0$ increase and regular fluctuations, experimental SEM and numerical FEA simulations were conducted. After cyclic bending of 10000 cycles, both metal-FPI and PMP present a lot of microcracks normal to bending direction (**Fig. 5c, e**), which should be responsible for the resistance increase. When releasing back to planar state, the developed microcracks for both specimens recover partially (**Fig. S5b, d**), thus generating regular fluctuations for each bending cycle. Noticeably, the width of cracks in metal-FPI can reach 10 μm or more (**Fig. S5a**), while much smaller microcracks develop in PMP interconnector at the same bending state. Based upon Kirchhoff 's Current Law, grayscale SEM images were turned into binary, the voltage distribution was estimated with applying a voltage drop of 1V on the left and right sides.[34, 35] It is clearly shown that the voltage distribution of metal-FPI is significantly disturbed by big cracks and voltages drops fast when encountering big cracks. Nevertheless, that of PMP interconnector is more even and the voltage drop is little affected by smaller and shorter microcracks, representing a smaller resistance change under bending (**Fig. 5f**). The FEA simulation results are well in agreement with experimental results. Brittle metals are not capable of bearing large strain and once microcracks are formed. These microcracks will propagate rapidly and irreversibly under the stress field of bending. Due to the greater toughness of parylene than metals and the hierarchical construction, the compact and thin parylene film assists PMP interconnector in alleviating the bending stress and increasing its resistance to deformation, which hinders the formation of micro-cracks and slows down the rate of propagation. As a positive consequence, PMP interconnector shows superior bending durability with a slight increase of $\Delta R/R_0$. Such enhanced abrasion resistance and cyclic bending durability bestow PMP interconnector desirable and satisfactory electro-mechanical stability for wearable applications.

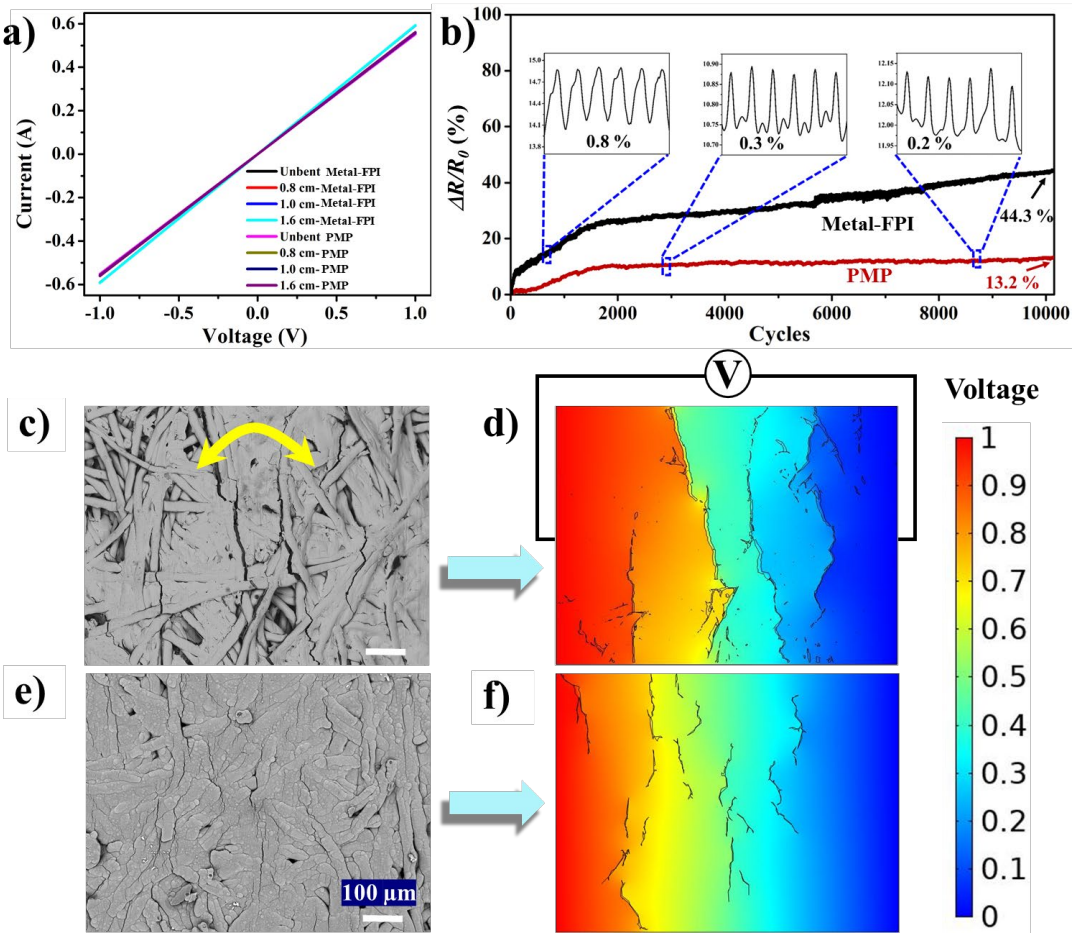

Fig. 5. Bending reliability. (a) I-V characteristics at different bending radii (0.8, 1.0 and 1.6 cm) and unbent state. The gauge length is 4 cm. (b) $\Delta R/R_0$ against bending cycles for metal-FPI and PMP. (c, e) SEM images of microcracks development at maximum curvature state after 10000 bending cycles for metal-FPI (c) and PMP (e). (d, f) Voltage distribution by FEA simulation, based on corresponding SEM images of (c) and (e).

3.4 Machine-washability

Machine-washability is also a very crucial factor to determine wearable electronics' applications. Many kinds of wearable electronics have been widely developed and well documented.[36] However, there are only a few successful cases of smart electronics into practical applications and industrialization because of poor washability. Water invasion and corrosion can severely degrade electrical performance, even resulting in direct failure. During washing, many kinds of mechanical actions, like bending, twisting, rubbing, stretching, can further cause serious damage.[37] The washability of wearable technology is a long-standing

concern but still unresolved problem. Here we envisage that parylene encapsulating layer could also exert a positive impact on the washability of PMP interconnector based on not only enhanced electro-mechanical stability but also inherently excellent waterproof properties of parylene.

In order to estimate the machine-washing stability of metal-FPI and PMP interconnector, the $\Delta R/R_0$ with washing cycles have been plotted in **Fig. 6a**. The result demonstrates that $\Delta R/R_0$ of metal-FPI increases by 300 times after only 12 washing cycles, while that of PMP interconnector experiences a slight increase of 1.2 times for 50 washing cycles. This is desirable and satisfactory in most wearable applications.[38, 39] The optical image and SEM image of metal-FPI after 12 washing cycles shows the failure of metal layer and loose fiber structure (**Fig. 6b and Fig. S6a**). In comparison, the metal layer and the fibrous structure of PMP interconnector keep almost intact after 50 washing cycles (**Fig. 6d and Fig. S6b**). In fact, the increased resistance of PMP interconnector mainly results from the unencapsulated edge for connecting power supply (**Fig. S6c**). It means that the shedding of metals and the mechanical damage of FPI membrane lead to the unstable resistance and final failure of conductive network in metal-FPI due to intense water invasion and corrosion as well as multi-mechanical destruction. EDS spectrum of metal-FPI demonstrates that Ni/Cu ratio decreases sharply after washing (inserted bar graph in **Fig. 6c**). However, that of PMP interconnector maintains almost the same after 50 washing cycles in **Fig. 6e**, saliently manifesting its superb washability and stability. Good machine washability requires encapsulated interconnector not only to be highly waterproof but also to be mechanically robust and durable. As aforementioned, PMP interconnector exhibits outstanding electro-mechanical robustness. Beyond that, parylene has been reported to own superior water resistance ability in the static case due to high-crystallinity, pinhole-free, and conformally protective structure.[40] Naked metal-FPI is vulnerable to dynamic water intrusion when washing (**Fig. 6b**). By virtue of superior waterproof trait and enhanced electro-mechanical durability, PMP interconnector maintains complete conductive network and functions well after 50 washing cycles. A comparison of $\Delta R/R_0$ versus machine washing cycles among different machine-washable electronics has been drawn in **Fig. 6g**. [24, 25, 39, 41-51] It is distinctly seen that most of wearable electronics demonstrate inferior machine washability at the top left of the graph, that is, low machine-washing cycles but high relative resistance change. Nevertheless, this work achieves high machine-washing capacity and fills the vacancy in bottom right corner of the graph. Moreover, it is noteworthy that, in comparison with the mostly reported film-based interconnectors, the novel PMP interconnector with interlaced fibers not only owns ample air-permeability, but also particular merits of tear strength to prevent catastrophic failure.[52] By virtue of porous high-performance substrate and ubiquitous parylene encapsulation, this work provides a facile and effective

method to fabricate comfort and stable interconnector with high conductivity, electro-mechanical durability and washability, guaranteeing the reliability for long-term wearable applications.

Different from the $\Delta R/R_0$ change during machine-washing, which mainly results from water invasion, mechanic agitation, and the metals shedding of PMP interconnector in the unencapsulated edge, perspiration wet-dry cycles come from chemical corrosion and oxidation instead of mechanical deformations. Herein, the PMP interconnector are immersed in synthetic perspiration with wet-dry cycles. After each drying, corresponding $\Delta R/R_0$ is recorded as shown in **Fig. 6f**. The extracted $\Delta R/R_0$ data within 1 can be highly linear fitting according to oxidation kinetics, as shown by equation (1), where t is time, k and C are constants. This analysis has been used frequently to estimate the oxidation of Cu.[53, 54]

$$\Delta R/R_0 = kt + C \qquad (1)$$

If we define the times at which $\Delta R/R_0 = 1$ as lifetime (τ), the immersing perspiration cycles of metal-FPI and PMP interconnector are 9 and 21 times, respectively. That means perspiration lifetime of PMP interconnector can reach about 100 hours, demonstrating significantly improved perspiration resistance. Obvious metal corrosion of metal-FPI can be observed in **Fig. 6h** due to oxidation by exposure in the artificial sweat solution with chemically aggressive sodium chloride, sodium hydroxide and lactic acid (**Fig. S7**). The metal corrosion process leads to the linear increase of electrical resistance. With the protection of parylene, the metal corrosion has been retarded obviously in PMP interconnector.

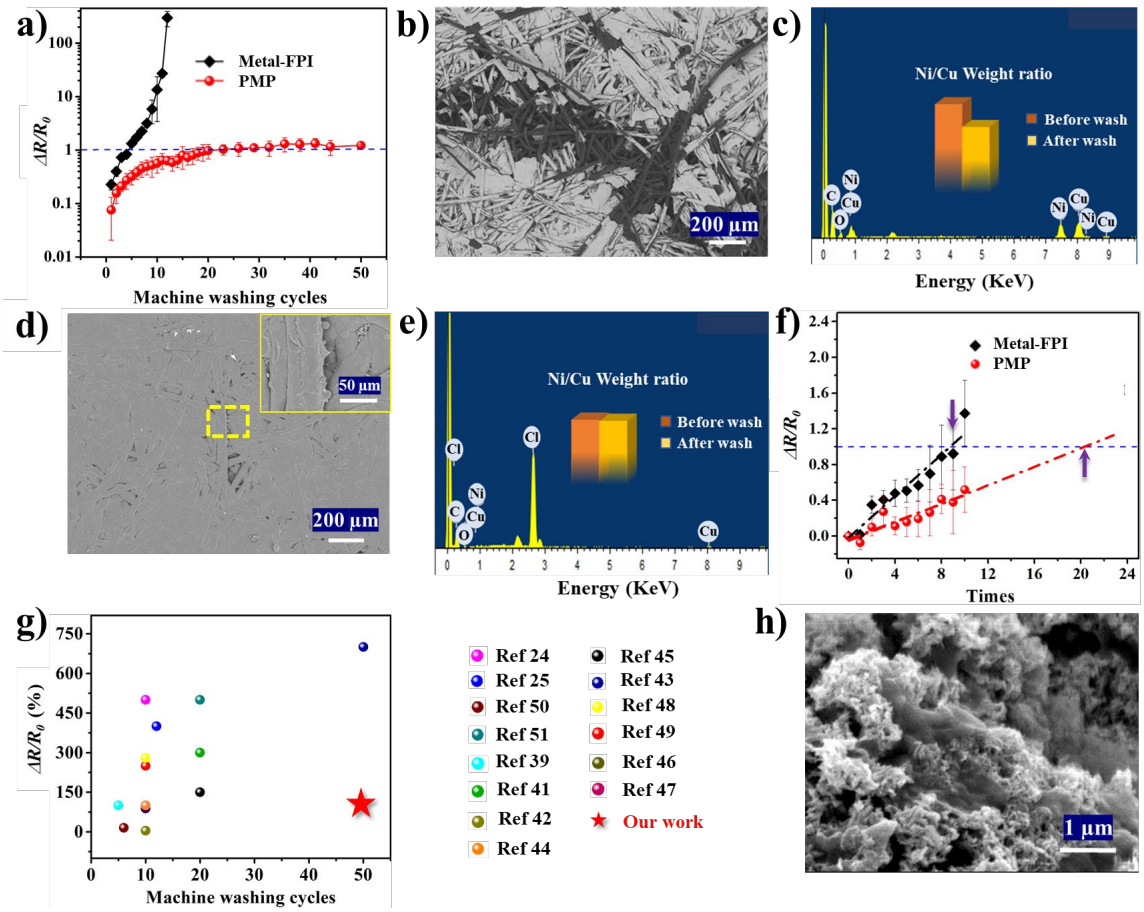

Fig. 6. The washability and perspiration resistance. (a) Normalized resistance against machine washing cycles. (b) SEM surface morphology of metal-FPI after washing 12 times. (c) The EDS spectrum of metal-FPI after washing and corresponding weight ratio change of Ni/Cu in inserted column. (d) SEM surface morphology of PMP after washing 50 times. (e) The EDS spectrum of PMP after washing and corresponding weight ratio change of Ni/Cu in inserted column. (f) Normalized resistance against perspiration wet-dry cyclic times. (g) Relative resistance changes versus machine washing cycles for the comparison of machine-washable electronics. (h) SEM image of local corrosion in metal-FPI.

3.4 Wearable electronics application

This newly PMP interconnector demonstrates decent air-permeability, excellent conductivity, great electro-mechanical durability, superb machine-washability and perspiration resistance, showing excellent potential in wearable electronics. On this basis, we further designed flexible circuit board (FCB) to support the integrated circuits and connect different electronic components, which is indispensable for flexible electronic devices.[55] More importantly, taking advantage of excellent tailorability, miniaturized FCB is

expected to be integrated into textile by braiding or weaving, conformally fitting into arbitrarily curved human body. Herein, FCB based on FPI membrane was prepared by an additive manufacturing,[56] including patterning and electroless plating as well as electroplating procedure as described in the experiment section. High-resolution circuit tracks with 700 μm width are observed in **Fig. S8a**. LEDs were surface mounted on thermally stable FPI membrane. The strong wet strength and high degradation temperature of FPI membrane empower strong endurance of the additive manufacturing process and the high soldering temperature. Finally, the FPI-based electronics were accomplished by parylene encapsulation, which was applied at extreme working environments. Initially, the weather resistance of wearable electronics was evaluated by exposing in seawater, hot water as well as ice. The wearable electronics can work stably more than 7 days soaked in seawater and its working current keeps unchanged during this period of time (**Fig. 7a**). The lifespan of the FPI-based electronics can extend even more than 30 days in deionized water (**Fig. S9d**). More importantly, the wearable electronics exhibit excellent stability even in boiling and ice water for 2 hours (**Fig. 7b** and **c**), clearly indicating they are fully competent in both extremely high and low temperatures with desirable waterproof properties. In a sharp contrast, if not encapsulated, the LED lights get off immediately upon the exposure to seawater (**Video S1**), and strong galvanic corrosion and lots of bubbles happen in the exposed circuits (**Figure S9**).

An infrared thermal camera was employed to capture the heating change of the wearable electronics under continuous working state. Three random LEDs on electronics show almost the same level of temperature (**Fig. 7d**), suggesting similar heat dissipation. With continuous lighting in 90 days, one LED of wearable electronics has been recorded and demonstrates stable heating temperature. Notably, encapsulated electronics shows the same trend with that of naked one. Apparently thin parylene layer of electronics exerts little influence on the thermal dissipation lasting 90 days (**Fig. 7e**) due to its small thickness of several micrometers. Moreover, both the two circuits display facile working temperature lower than 39 °C, which will guarantee these FPI-based electronics users friendly when in close contact with human skins. Although circuit tracks are fine and surface-mounted with LEDs, such wearable electronics show notable bending stability and high flexibility. The corresponding luminance maintains unchanged beyond 3000 bending cycles (**Fig. 7f**).

To demonstrate the scale controllability and e-textile applications, the as-mentioned flexible FPI-based electronics are capable of tailoring into core yarns, which were spun into yarns with polyethylene as loading yarn and nylon 6 as cover yarn. Furthermore, the electronic yarns can be braided as wearable bracelet or be woven into fabrics by weaving machine as exhibited in **Fig. 7g**. Waterproof parylene encapsulation and

reasonable yarn-making structure render the e-textile great washability. Hand washing has been conducted according to AATCC LP2-2018. The e-textile can withstand more than 50 washing cycles and maintain sound working state (**Fig. 7h**). Such highly flexible, breathable, well insulated, and stable electronic yarns can be easily integrated into fabrics by weaving or knitting machines for broad wearable applications. For example, a raincoat with the integrated electronic yarns can work steadily for several hours under heavy rain as shown in **Fig. 7i** and **video S2**, which can assist traffic police in conducting the traffic under rainy days. Even more, the life vest integrated with durable electronics can increase the survival chances of escape when trapped at sea or harsh environment. The air permeability of fabrics has been conducted considering of the comfort issues.[57] The specific airflow resistance is about 0.127 KPa*s/m. The result shows there is little influence on air permeability of the fabric after integrating FCB (**Table S2**). Such strategy of integration of electronic yarns with textile exerts little influence on the aesthetic beauty and comfortable wearing, showing huge potential for wearable electronics applications. While the cost of FPI membrane and the limited length of the interconnector would be the reasons of restricting their scaleup production. More efforts will be made to solve these problems. Besides, this stable and washable interconnector is expected to accommodate more microelectronics, thus greatly broadening their wearable applications.

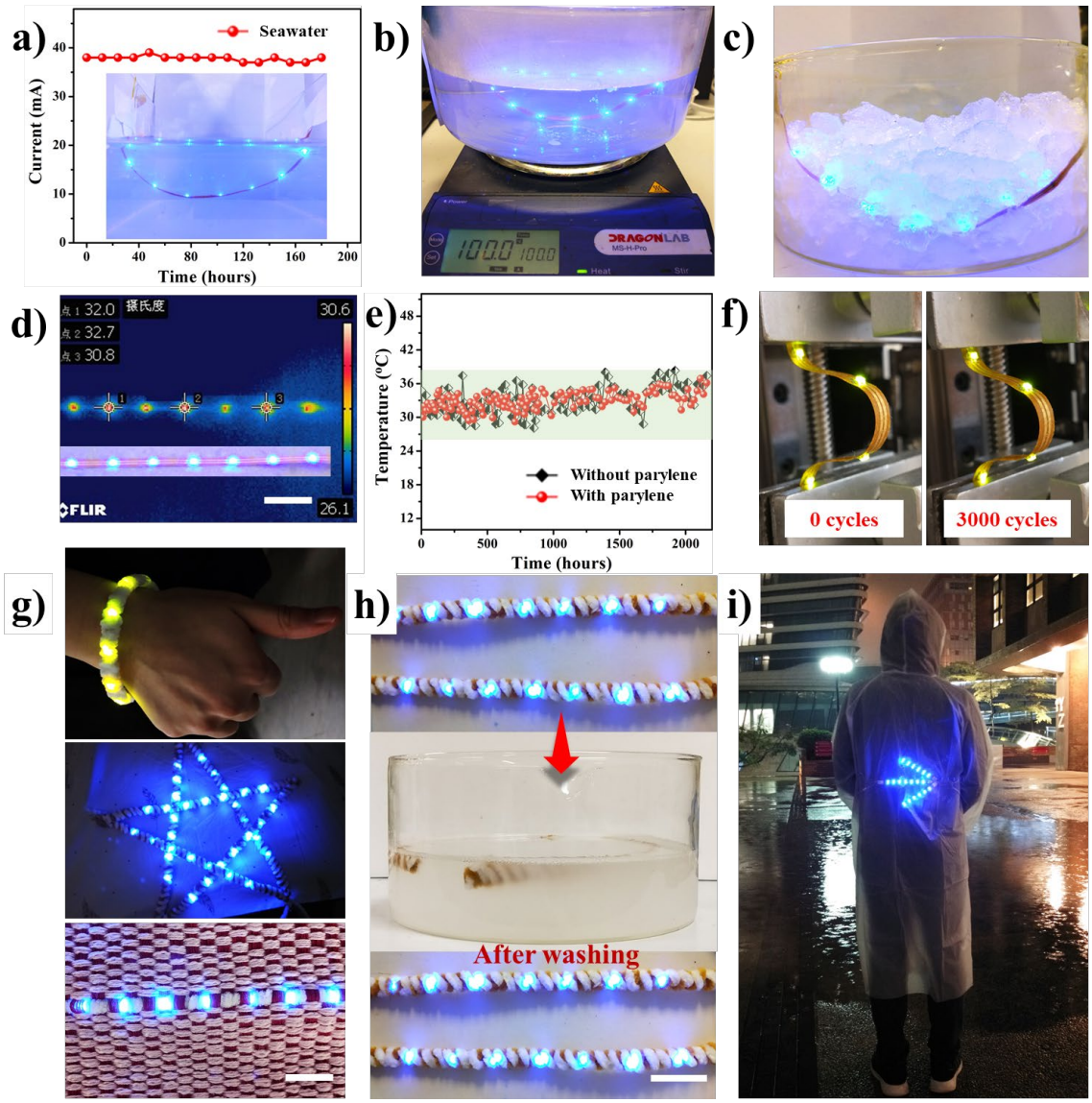

Fig. 7. Weather resistance and applications of FPI-based electronics. (a) The resistance-time curve of FPI-based electronics immersed into seawater lasting 7 days. Insert picture is lighting state after 7 days. (b, c) Weather stability of FPI-based electronics under boiling water and ice. (d) FLIR image of wearable electronics. (e) The heating stability of FPI-based electronics under working state lasting 90 days. (f) The luminance of FPI-based electronics before and after 3000 bending cycles. The bending radius is 1.0 cm. (g) Photographs of FPI-based electronics braided into wearable bracelet after yarn spinning or woven into fabrics by weaving machine. (h) The washability of electronic yarns. (i) Electronic textile integrated with FPI-based electronics served as wearable traffic arrow under rainy days. The scale bar is 2 cm.

4. Conclusion

In this work, we have designed a newly permeable, stable and washable interconnector, with FPI membrane as substrate, Cu/Ni multilayer as conductive layer, and parylene as robust encapsulation. Arising from porous FPI membrane and ubiquitous parylene encapsulation, the resultant parylene-metal-FPI (PMP) interconnector displays decent air-permeability and notable conductivity. It possesses supreme abrasive endurability, with only 2.2 % mass loss and little Ni/Cu weight ratio change beyond 50000 abrasion cycles. After 10000 dynamic bending-releasing cycles, PMP interconnector shows only 13.1 % relative resistance increase, exhibiting an excellent electro-mechanical stability. Moreover, the machine washability (50 times) and perspiration resistance (beyond twice) of PMP interconnector have been improved enormously for the first time. In addition, as a proof of concept, a flexible circuit board assembly was further fabricated by soldering a series of LEDs on the interconnectors, followed by parylene encapsulation. The as-fabricated electronics show superior lifespan in harsh environment (seawater, ice, boiled water, and heavy rain), which can be further spun into yarns and woven into fabrics with aesthetic beauty and comfortable wearing. Of particular note, this work provides a facile and effective method to fabricate comfort and stable interconnector with high conductivity, electro-mechanical durability and washability, guaranteeing the reliability for long-term wearable application and showing great possibility for high-throughput production. Furthermore, this stable and washable interconnector is expected to accommodate more microelectronics, thus greatly broadening their wearable applications.

Associated Content

Supporting Information

Additional data for parylene encapsulation process, physical properties of polyimide membrane, EDS mapping, FTIR, TGA data, peeling strength, optical images and SEM images after washing, sweat test, and bending test. Waterproof properties and air permeability impedance for FPI-based circuit board.

Author Information

Corresponding Author

xiao-ming.tao@polyu.edu.hk

ORCID

Xiao-ming Tao: 0000-0002-2406-0695

Notes

The authors declare no competing financial interest.

Acknowledgement

This research has been partially supported by the Research Grants Council of Hong Kong, China (Project No.15200917E), Innovation and Technology Commission (No. ITS/306/17), Endowed Professorship Fund, The Hong Kong Polytechnic University (No.847A), and postgraduate scholarships by the Hong Kong Polytechnic University. We thank the technicians Mr. Vincent Tang, Mr. TL Yip, Mr. CW Lee, Mr. YC Tam from Industrial Center of Hong Kong Polytechnic University for the technical support on circuit board fabrication.

References

1. Shi J, Liu S, Zhang L, Yang B, Shu L, Yang Y, Ren M, Wang Y, Chen J, Chen W, Chai Y, Tao X. Smart Textile-Integrated Microelectronic Systems for Wearable Applications. Adv Mater 2020**,** 32 (5), e1901958.
2. Honda W, Harada S, Arie T, Akita S, Takei K. Wearable, Human-Interactive, Health-Monitoring, Wireless Devices Fabricated by Macroscale Printing Techniques. Adv Funct Mater 2014**,** 24 (22), 3299-304.
3. He Y, Zhao L, Zhang J, Liu L, Liu H, Liu L. A breathable, sensitive and wearable piezoresistive sensor based on hierarchical micro-porous PU@ CNT films for long-term health monitoring. Compos Sci Technol 2020**,** 200, 108419.
4. Tao X, *Handbook of smart textiles*. Springer Singapore: 2015.
5. Lee J, Kwon H, Seo J, Shin S, Koo J H, Pang C, Son S, Kim J H, Jang Y H, Kim D E, Lee T. Conductive fiber-based ultrasensitive textile pressure sensor for wearable electronics. Adv Mater 2015**,** 27 (15), 2433-9.
6. Zhu M, Wang Y, Lou M, Yu J, Li Z, Ding B. Bioinspired transparent and antibacterial electronic skin for sensitive tactile sensing. Nano Energy 2021**,** 81, 105669.
7. Song P, He X, Xie M, Tao J, Shen X, Ji Z, Yan Z, Zhai L, Yuan A. Polyaniline wrapped graphene functionalized textile with ultrahigh areal capacitance and energy density for high-performance all-solid-state supercapacitors for wearable electronics. Compos Sci Technol 2020**,** 198, 108305.
8. Gupta S, Chang C, Anbalagan A K, Lee C-H, Tai N-H. Reduced graphene oxide/zinc oxide coated wearable electrically conductive cotton textile for high microwave absorption. Compos Sci Technol 2020**,** 188, 107994.
9. de Mulatier S, Nasreldin M, Delattre R, Ramuz M, Djenizian T. Electronic circuits integration in textiles for data processing in wearable technologies. Adv Mater Technol 2018**,** 3 (10), 1700320.

10. Ji D, Li T, Hu W, Fuchs H. Recent progress in aromatic polyimide dielectrics for organic electronic devices and circuits. Adv Mater 2019**,** 31 (15), 1806070.
11. Wang D, Zhang Y, Lu X, Ma Z, Xie C, Zheng Z. Chemical formation of soft metal electrodes for flexible and wearable electronics. Chem Soc Rev 2018**,** 47 (12), 4611-41.
12. Wang J, Chen Y, An J, Xu K, Chen T, Müller-Buschbaum P, Zhong Q. Intelligent textiles with comfort regulation and inhibition of bacterial adhesion realized by cross-linking poly (n-isopropylacrylamide-co-ethylene glycol methacrylate) to Cotton Fabrics. ACS Appl Mater Interfaces 2017**,** 9 (15), 13647-56.
13. Niu B, Hua T, Xu B. Robust Deposition of Silver Nanoparticles on Paper Assisted by Polydopamine for Green and Flexible Electrodes. ACS Sustainable Chem. Eng. 2020**,** 8 (34), 12842-51.
14. Wu C, Kima T W, Sung S, Park J H, Li F. Ultrasoft and cuttable paper-based triboelectric nanogenerators for mechanical energy harvesting. Nano Energy 2018**,** 44, 279-87.
15. Siegel A C, Phillips S T, Dickey M D, Lu N, Suo Z, Whitesides G M. Foldable printed circuit boards on paper substrates. Adv Funct Mater 2010**,** 20 (1), 28-35.
16. Yang W, Cao R, Zhang X, Li H, Li C. Air‐Permeable and Washable Paper‐Based Triboelectric Nanogenerator Based on Highly Flexible and Robust Paper Electrodes. Adv Mater Technol 2018**,** 3 (11), 1800178.
17. Tobjork D, Osterbacka R. Paper electronics. Adv Mater 2011**,** 23 (17), 1935-61.
18. Saetia K, Schnorr J M, Mannarino M M, Kim S Y, Rutledge G C, Swager T M, Hammond P T. Spray‐layer‐by‐layer carbon nanotube/electrospun fiber electrodes for flexible chemiresistive sensor applications. Adv Funct Mater 2014**,** 24 (4), 492-502.
19. Gao J, Li B, Huang X, Wang L, Lin L, Wang H, Xue H. Electrically conductive and fluorine free superhydrophobic strain sensors based on SiO2/graphene-decorated electrospun nanofibers for human motion monitoring. Chem Eng J 2019**,** 373, 298-306.
20. Li B, Luo J, Huang X, Lin L, Wang L, Hu M, Tang L, Xue H, Gao J, Mai Y-W. A highly stretchable, super-hydrophobic strain sensor based on polydopamine and graphene reinforced nanofiber composite for human motion monitoring. Composites Part B: Engineering 2020**,** 181, 107580.
21. Xu S, Zhang Y, Jia L, Mathewson K E, Jang K-I, Kim J, Fu H, Huang X, Chava P, Wang R. Soft microfluidic assemblies of sensors, circuits, and radios for the skin. Science 2014**,** 344 (6179), 70-74.
22. Russo A, Ahn B Y, Adams J J, Duoss E B, Bernhard J T, Lewis J A. Pen‐on‐paper flexible electronics. Adv Mater 2011**,** 23 (30), 3426-30.
23. Liu H, Jiang H, Du F, Zhang D, Li Z, Zhou H. Flexible and degradable paper-based strain sensor with low cost. ACS Sustainable Chem. Eng. 2017**,** 5 (11), 10538-43.
24. Zhao Z, Huang Q, Yan C, Liu Y, Zeng X, Wei X, Hu Y, Zheng Z. Machine-washable and breathable pressure sensors based on triboelectric nanogenerators enabled by textile technologies. Nano Energy 2020**,** 70, 104528.
25. Zhao Z, Yan C, Liu Z, Fu X, Peng L M, Hu Y, Zheng Z. Machine‐washable textile triboelectric nanogenerators for effective human respiratory monitoring through loom weaving of metallic yarns. Adv Mater 2016**,** 28 (46), 10267-74.
26. Lou M, Abdalla I, Zhu M, Wei X, Yu J, Li Z, Ding B. Highly wearable, breathable, and washable sensing textile for human motion and pulse monitoring. ACS Appl Mater Interfaces 2020**,** 12 (17), 19965-73.
27. Ryan J D, Mengistie D A, Gabrielsson R, Lund A, Müller C. Machine-washable PEDOT: PSS dyed silk yarns for electronic textiles. ACS Appl Mater Interfaces 2017**,** 9 (10), 9045-50.
28. Niu B, Yang S, Hua T, Tian X, Koo M. Facile fabrication of highly conductive, waterproof, and washable e-textiles for wearable applications. Nano Research 2020, 1-10.
29. Sudagar J, Lian J, Sha W. Electroless nickel, alloy, composite and nano coatings–A critical review. J Alloys Compd 2013**,** 571, 183-204.

30. Song C H, Choi Y, Lee J-Y, Kim M. Electro-magnetic insulating behavior of thin multilayered copper-nickel composite mesh sheet formed by two-step pulse electroplating. The Physics of Metals and Metallography 2014**,** 115 (13), 1275-80.
31. Lecomte A, Descamps E, Bergaud C. A review on mechanical considerations for chronically-implanted neural probes. Journal of neural engineering 2018**,** 15 (3), 031001.
32. Bansal A, Zafar S, Sharma A K. Microstructure and abrasive wear performance of Ni-WC composite microwave clad. J Mater Eng Perform 2015**,** 24 (10), 3708-16.
33. Liao X, Liao Q, Yan X, Liang Q, Si H, Li M, Wu H, Cao S, Zhang Y. Flexible and highly sensitive strain sensors fabricated by pencil drawn for wearable monitor. Adv Funct Mater 2015**,** 25 (16), 2395-401.
34. Jiang Y, Liu Z, Matsuhisa N, Qi D, Leow W R, Yang H, Yu J, Chen G, Liu Y, Wan C. Auxetic mechanical metamaterials to enhance sensitivity of stretchable strain sensors. Adv Mater 2018**,** 30 (12), 1706589.
35. Cao W, Görrn P, Wagner S. Modeling the electrical resistance of gold film conductors on uniaxially stretched elastomeric substrates. Appl Phys Lett 2011**,** 98 (21), 212112.
36. Stoppa M, Chiolerio A. Wearable electronics and smart textiles: a critical review. Sensors (Basel) 2014**,** 14 (7), 11957-92.
37. Zeng W, Shu L, Li Q, Chen S, Wang F, Tao X M. Fiber-based wearable electronics: a review of materials, fabrication, devices, and applications. Adv Mater 2014**,** 26 (31), 5310-36.
38. Ankhili A, Tao X, Cochrane C, Coulon D, Koncar V. Washable and Reliable Textile Electrodes Embedded into Underwear Fabric for Electrocardiography (ECG) Monitoring. Materials (Basel) 2018**,** 11 (2), 256.
39. Tao X Y, Koncar V, Huang T H, Shen C L, Ko Y C, Jou G T. How to Make Reliable, Washable, and Wearable Textronic Devices. Sensors 2017**,** 17 (4), 673.
40. Tan C P, Craighead H G. Surface engineering and patterning using parylene for biological applications. Materials 2010**,** 3 (3), 1803-32.
41. Choi B, Lee J, Han H, Woo J, Park K, Seo J, Lee T. Highly Conductive Fiber with Waterproof and Self-Cleaning Properties for Textile Electronics. ACS Appl Mater Interfaces 2018**,** 10 (42), 36094-101.
42. Zaman S, Tao X, Cochrane C, Koncar V In *Market readiness of smart textile structures-reliability and washability*, IOP Conference Series: Materials Science and Engineering, IOP Publishing: 2018; p 012071.
43. Afroj S, Karim N, Wang Z, Tan S, He P, Holwill M, Ghazaryan D, Fernando A, Novoselov K S. Engineering graphene flakes for wearable textile sensors via highly scalable and ultrafast yarn dyeing technique. Acs Nano 2019**,** 13 (4), 3847-57.
44. Zhou X, Zhu L, Fan L, Deng H, Fu Q. Fabrication of highly stretchable, washable, wearable, water-repellent strain sensors with multi-stimuli sensing ability. ACS Appl Mater Interfaces 2018**,** 10 (37), 31655-63.
45. Vervust T, Buyle G, Bossuyt F, Vanfleteren J. Integration of stretchable and washable electronic modules for smart textile applications. Journal of the Textile Institute 2012**,** 103 (10), 1127-38.
46. Rotzler S, Kallmayer C, Dils C, von Krshiwoblozki M, Bauer U, Schneider-Ramelow M. Improving the washability of smart textiles: influence of different washing conditions on textile integrated conductor tracks. The Journal of The Textile Institute 2020, 1-12.
47. Karim N, Afroj S, Tan S, He P, Fernando A, Carr C, Novoselov K S. Scalable production of graphene-based wearable e-textiles. ACS nano 2017**,** 11 (12), 12266-75.
48. Huang T, Zhang J, Yu B, Yu H, Long H, Wang H, Zhang Q, Zhu M. Fabric texture design for boosting the performance of a knitted washable textile triboelectric nanogenerator as wearable power. Nano Energy 2019**,** 58, 375-83.
49. Carey T, Cacovich S, Divitini G, Ren J, Mansouri A, Kim J M, Wang C, Ducati C, Sordan R, Torrisi F. Fully inkjet-printed two-dimensional material field-effect heterojunctions for wearable and textile electronics. Nat Commun 2017**,** 8 (1), 1-11.

50. Jo K, Kim C-H, Won S, Hwangbo Y, Kim J-H, Lee H-J, Lee S-M. Calligraphic ink enabling washable conductive textile electrodes for supercapacitors. J Mater Chem A 2016**,** 4 (11), 4082-88.
51. Tang Z, Yao D, Du D, Ouyang J. Highly machine-washable e-textiles with high strain sensitivity and high thermal conduction. J Mater Chem C 2020.
52. Zeng W, Shu L, Li Q, Chen S, Wang F, Tao X M. Fiber‐based wearable electronics: a review of materials, fabrication, devices, and applications. Adv Mater 2014**,** 26 (31), 5310-36.
53. Rathmell A R, Nguyen M, Chi M, Wiley B J. Synthesis of oxidation-resistant cupronickel nanowires for transparent conducting nanowire networks. Nano Lett 2012**,** 12 (6), 3193-99.
54. Song J, Li J, Xu J, Zeng H. Superstable transparent conductive Cu@ Cu4Ni nanowire elastomer composites against oxidation, bending, stretching, and twisting for flexible and stretchable optoelectronics. Nano Lett 2014**,** 14 (11), 6298-305.
55. Liu J, Yang C, Wu H, Lin Z, Zhang Z, Wang R, Li B, Kang F, Shi L, Wong C P. Future paper based printed circuit boards for green electronics: fabrication and life cycle assessment. Energ Environ Sci 2014**,** 7 (11), 3674-82.
56. Gao W, Zhang Y, Ramanujan D, Ramani K, Chen Y, Williams C B, Wang C C, Shin Y C, Zhang S, Zavattieri P D. The status, challenges, and future of additive manufacturing in engineering. Computer-Aided Design 2015**,** 69, 65-89.
57. Gu P, Fan N, Wang Y, Wang J, Müller-Buschbaum P, Zhong Q. Linear control of moisture permeability and anti-adhesion of bacteria in a broad temperature region realized by cross-linking thermoresponsive microgels onto cotton fabrics. ACS Appl Mater Interfaces 2019**,** 11 (33), 30269-77.